Journal of Molecular Liquids xxx (xxxx) xxx

Contents lists available at ScienceDirect

Journal of Molecular Liquids

journal homepage: www.elsevier.com/locate/molliq

Structure and vibrational features of the protic ionic liquid 1,8-diazabicyclo[5.4.0]-undec-7-ene-8-ium bis(trifluoromethanesulfonyl) amide, [DBUH][TFSI]

Alessandro Triolo [a,*], Annalisa Paolone [b,*], Angelo Sarra [b], Francesco Trequattrini [b,c], Oriele Palumbo [b], Giovanni BattistaAppetecchi [d], Fabrizio Lo Celso [a,e], Philip Chater [f], Olga Russina [a,g,*]

[a] Laboratorio Liquidi Ionici, Istituto Struttura della Materia, Consiglio Nazionale delle Ricerche, (ISM-CNR), Rome, Italy
[b] Consiglio Nazionale delle Ricerche, Istituto dei Sistemi Complessi, Piazzale A. Moro 5, 00185 Roma, Italy
[c] Department of Physics, Sapienza University of Rome, Piazzale A. Moro 5, 00185 Roma, Italy
[d] ENEA, SSPT-PROMAS-MATPRO Technical Unit, Rome, Italy
[e] Department of Physics and Chemistry, Università di Palermo, Palermo, Italy
[f] Diamond House, Harwell Science & Innovation Campus, Diamond Light Source, Ltd., Didcot, UK
[g] Department of Chemistry, University of Rome Sapienza, Rome, Italy

ARTICLE INFO

Article history:
Received 28 July 2021
Revised 12 October 2021
Accepted 26 October 2021
Available online xxxx

Keywords:
Protic Ionic Liquid
Hydrogen bonding
X-ray scattering
Far-ir spectroscopy
Molecular Dynamics
DFT calculation

ABSTRACT

The Protic Ionic Liquid (PIL) formed by neutralization of the super-strong base 1,7-diazabicyclo[5.4.0]undec-7-ene (DBU) with the super-strong acid bis(trifluoromethanesulfonyl)-imide (TFSI), indicated as [DBUH][TFSI], has been investigated. Its chemical physical properties and structural features have been explored using a synergy of experimental and computational tools. Molecular Dynamics-rationalised X-ray diffraction patterns highlight the major role played by hydrogen bonding (HB) in affecting morphology in this PIL. A comparison between HB features in this and in related PILs has been presented, on the base of far-IR experiments and DFT analysis. Indications of a weaker HB interaction in [DBUH][TFSI] in comparison with [DBUH][TfO], consistently with their ΔpK_a difference, have been observed and rationalised in terms of geometrical properties of the main conformers contributing to the experimental spectra. In the liquid phase of [DBUH][TFSI] a particularly large conformational disorder is observed and the corresponding large dispersion of the frequencies of the HB stretching modes leads to a broad absorption band without a well defined peak. On the contrary, well detectable HB related absorptions are observable in the solid phase of [DBUH][TFSI] and at all temperatures in [DBU][TfO], where less configurational disorder occurs.

1. Introduction

Protic ionic liquids (PILs) represent an appealing class of compounds composed solely of ionic species, with melting point below 100 °C, which are characterised by proton transfer from an acidic to a basic species, thus leading to the establishment of an extended hydrogen bonding network [1]. In 1888, Gabriel reported the preparation of the first PIL compound: ethanolammonium nitrate (melting point: 52–55 °C) [2], while Walden discovered the first PIL in the liquid state at ambient conditions in 1914, namelyethylammonium nitrate (EAN, melting point: 12 °C) [3]. The opportunity provided by the presence of a transferrable proton opened the way to the proposal of PILs as appealing fuel cell electrolytes. [4,5] On the other hand the availability of proton in the bulk PIL depends on the difference between pKa values of the acid and base species determined in dilute aqueous solutions (hereinafter indicated as ΔpKa) [6]. Upon neutralization of the super-strong base 1,7-diazabicyclo[5.4.0]undec-7-ene (hereinafter indicated as DBU) with the super-strong acid, bis(trifluoromethanesulfonyl)amide acid (H[TFSI]), one derives the protic ionic liquid , [DBUH][TFSI], that is characterised by a record high $\Delta pK_a = 23.4$ (for comparison, Kanzaki et al. [7] reported EAN's $\Delta pK_a = 10$) [6,8-10]. DBU is a sterically hindered amidine, where the positive mesomeric effect of the adjacent nitrogen atom stabilizes the protonated species [11], only the imino nitrogen getting protonated [9]. We

* Corresponding authors at: Laboratorio Liquidi Ionici, Istituto Struttura della Materia, Consiglio Nazionale delle Ricerche, (ISM-CNR), Rome, Italy; Consiglio Nazionale delle Ricerche, Istituto dei Sistemi Complessi, Piazzale A. Moro 5, 00185 Roma, Italy; Department of Chemistry, University of Rome Sapienza, Rome, Italy
E-mail addresses: triolo@ism.cnr.it (A. Triolo), annalisa.paolone@roma1.infn.it (A. Paolone), olga.russina@uniroma1.it (O. Russina).

https://doi.org/10.1016/j.molliq.2021.117981
0167-7322/

recently reported on neat DBU structure, describing its local arrangement in the bulk liquid state [12]. In the past, related [DBUH]-based PILs have been studied by other groups. Tolstikova et al. prepared salts with Cl, Br, p-toluenesulfonate and triflate anions [13] and later with other fluorinated anions including [TFSI] [14], therein reporting preparation and solubility properties in diverse media, including water. The importance of the ΔpK_a parameter in determining key chemical-physical properties of PILs has been recently highlighted: Angell et al. proposed that ΔpK_a values>10 lead to substantial proton transfer and hence highly ionized PILs [6]. On the other hand, MacFarlane et al. proposed that a much lower value of ΔpK_a (>4) is required to achieve complete proton transfer. Watanabe et al. showed that values for ΔpK_a > 15 lead to PILs with enhanced thermal stability and high ionicity, due to the complete proton transfer and weak correlations between the charged species. [9]For smaller values, the large amount of neutral species and the establishment of hydrogen-bonding driven correlations between ions lead to low ionicity values. More recently, Miran et al. showed that when pairing super acid H[TFSI] with different strength bases (ranging from pyrazine to DBU), the threshold value for ΔpK_a to achieve thermally stable and high ionicity PILs is around 10, thus significantly dropping the value (such a result is supposedly due to the multiple proton donating and receiving site both in [TFSI] and in the cations) [10]. Here we are focusing on the PIL produced by neutralization of the super-strong base DBUwith the super-strong acid, H[TFSI]: accordingly the PIL [DBUH][TFSI] is characterised by complete proton transfer, very high thermal stability and ionicity. [9,10]

In this study, subsequent to a previous one from some of us that was focused on related [DBUH]-based PILs [12], we use experimental and computational techniques to explore the structural and vibrational features of [DBUH][TFSI]. Synchrotron high-energy X-ray diffraction is used to extract the liquid structure of the salt, thus complementing atomistic Molecular Dynamics simulations, accessing the local correlations between the different ions. In parallel, ab initio calculations are used to rationalise experimental far infrared spectroscopy data obtained at a synchrotron source, as a function of temperature. These highly complementary tools allow providing an accurate description of a very interesting PIL, where full proton transfer is considered to occur.

2. Experimental and computational section

2.1. Sample preparation

2.1.1. Synthesis of [DBUH][TFSI]

1,7-diazabicyclo[5.4.0]undec-7-ene (DBU) has been bought at TCI (Lot: YSUDE), with 99.4% purity. Before utilization it has been kept under vacuum for > 1 week and maintained in a moisture free environment.

The [DBUH][TFSI] (see Scheme 1) ionic liquid was synthesized by reacting the DBU strong base (previously diluted in deionized water according to a DBU:H_2O volume ratio equal to 1:1) with the stoichiometric amount of nitric acid (Sigma-Aldrich, 70 wt% in water solution). The DBU:HNO_3 mole ratio was fixed equal to 1:1 in order of achieve protonation of only one DBU N atom:

$$DBU + HNO_3 \rightarrow [DBUH][NO_3] \quad (1)$$

As the reaction (1) is rather exothermal, both reagents were previously cooled in a freezer before the synthesis. In addition, the (cold) aqueous HNO_3 solution was added dropwise to the (cold) DBU base and a water–ice bath was used to avoid uncontrolled temperature increase. Stirring was allowed for a few hours in order to bring the reaction to completeness. Then, lithium bis(trifluoro methylsulfonyl)-imide, LiTFSI (3 M, > 99.9 wt%), salt was added to the [DBUH][NO_3] solution, in order to obtain the [DBUH][TFSI] ionic liquid, according to the anion exchange reaction (2):

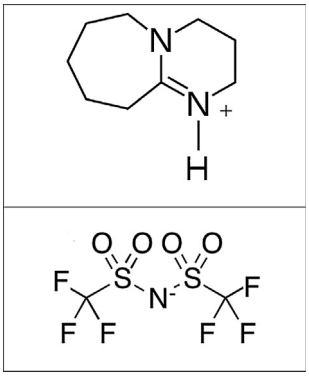

Scheme 1. Schematic representation of the ionic species composing the studied salt. On the top, the protonated form of 1,7-diazabicyclo[5.4.0]undec-7-ene ([$DBUH^+$]); on the bottom, the bis(trifluoro-methanesulfonyl) amide anion ([TFSI]) anions are shown.

$$[DBUH][NO_3] + LiTFSI \rightarrow [DBUH][TFSI] + LiNO_3 \quad (2)$$

LiTFSI was used in slight excess (2 wt%) with respect to the stoichiometric amount to maximise the reaction yield. [15] A fast formation of water-insoluble [DBUH][TFSI] as a solid precipitate was suddenly observed. Then, the system was stirred for one hour at room temperature[15] and, successively, kept at 5 °C to allow phase separation, i.e., the [DBUH][TFSI] lower solid phase (ionic liquid is denser than the water solution) and the aqueous upper phase (containing the $LiNO_3$ as the reaction by-product). The latter was removed by vacuum filtration, whereas [DBUH][TFSI] was repeatedly rinsed (five times) with deionized water (IL:H_2O volume ratio equal to 1:1) to remove the small fraction of $LiNO_3$ and LiTFSI dissolved in the ionic liquid and the water-soluble impurities. [15] Finally, the ionic liquid was vacuum dried according to the following protocol: room temperature (2 h), 50 °C (2 h) and 100 °C (24 h). The [DBUH][TFSI] material, housed within sealed glass containers, was stored and handled inan argon atmosphere glove box (H_2O and O_2 below 1 ppm). A moisture level below 2 ppm (determined by Karl-Fischer titration) was detected.

2.2. Conductivity measurements

The ionic conductivity of the [DBUH][TFSI] IL was determined through an AMEL 160 conductivity meter within the temperature range from −40 to 80 °C. The ionic liquid (solid at room temperature) was previously melt and, then, housed in sealed glass cells (AMEL 192/K1, cell constant equal to 1.00 ± 0.01 cm) equipped with two porous Pt electrodes. Successively, the cell was transferred in a climatic chamber (Binder GmbH MK53) at −40 °C. After a storage period at this temperature of 24 h, the conductivity of [DBUH][TFSI] was measured by running a heating scan at 1 °C h^{-1}.

2.3. High energy X-ray scattering

[DBUH][TFSI] was loaded into a borosilicate capillary of 1 mm outer diameter, which was glue-sealed. The total high-resolution X-ray scattering data were collected on the I15-1 beamline at Diamond Light Source, UK, using X-rays of wavelength 0.161669 Å (E = 76.69 keV) and a Perkin Elmer XRD 4343 CT detector. The total scattering data were integrated to 1D using DAWN [16] and then normalised and corrected to extract S(Q) using GudrunX [17,18].

2.4. Infrared absorbance measurements

The infrared absorbance spectrum of [DBUH][TFSI] was measured in the far-infrared range (35–680 cm^{-1}) as a function of temperature at the AILES beamline of Soleil Synchrotron. A Bruker IFS125 HR spectrometer, a bolometer detector and a Si/mylar beamsplitter were used to acquire data with a resolution of 1 cm^{-1}. The sample was preliminarily heated at ~ 350 K in order to have it in the liquid state, and a drop was placed between the diamond optical windows of a cell for liquids, equipped with O-rings to avoid contaminations from water and/or air. A mylar spacer, 50 μm thick, assured the proper thickness to highlight the absorbance bands occurring below 200 cm^{-1}. The cell temperature was varied by means of a Cryomec cryostat, starting at 330 K and cooling down to 160 K with a temperature rate of 5 K/min. Further measurements were acquired on heating back up to 340 K.

2.5. Molecular dynamics simulations

Molecular dynamic simulations were performed using the GROMACS 5.1.1 package [19,20]. Bonded and non bonded parameters for the TFSI anion were described using an all-atoms potential [21,22], while for the DBUH cation bonded parameters were obtained from ATB repository [23] (ATB molid: 306726; all-atoms topology); non bonded parameters for the cation were obtained from OPLS-AA force field [24]. The simulation for [DBUH][TFSI] salt was performed using a cubic box of 1500 ion pairs; periodic boundary conditions were applied. Force field parameter files for the anions were created by DLPGEN software [25] (http://webpages.fc.ul.pt/~cebernardes/dlpgen_prog/Software_dlpgen.html; accessed in march 2019); initial configurations were created by Packmol software [26]. The starting density was fixed 10 %higher than the experimental one. The equilibration procedure was performed in several steps, starting from a NVT simulation at 400 K and scaled partial charges (10% of the original ones), followed by a series of NPT runs lowering progressively the temperature (from 400 K to 350 K) and increasing the charges to their final value at 300 K and 1 bar, after a 10 ns run. This procedure was repeated two further times until an equilibrated system was obtained. After the equilibration phase, the system was run for a total of 50 ns for a production run, and then the trajectory of the last 5 ns was saved at a frequency of 1 ps for calculation of the structural properties. The simulations were always checked versus the experimental density and the energy profile. During the production runs for the temperature coupling, we used a velocity rescaling thermostat [27] (with a time coupling constant of 0.1 ps), while for the pressure coupling, we used a Parrinello–Rahman barostat [28] (1 ps for the relaxation constant). The Leap-Frog algorithm with a 1 fs time step was used for integrating the equations of motion. Cut-offs for the Lennard-Jones and real space part of the Coulombic interactions were set to 15 Å. For the electrostatic interactions, the Particle Mesh Ewald (PME) summation method [29,30] was used, with an interpolation order of 6 and 0.08 nm of FFT grid spacing. Selected graphs were produced using Matplotlib [31] and VMD [32]. Weighted and partial structure factors were computed by using in-house developed software, accordingly to text book formulas as highlighted in Margulis's work [33], while selected pair correlation function and angular distribution function were obtained by TRAVIS. [34-36]

2.6. DFT Calculations

DFT calculations were performed by means of the Spartan software [37]. Preliminary possible geometries of the [DBUH][TFSI] and [DBUH][TfO] ionic couples were generated at the molecular mechanics level, by a systematic rotations of flexible bonds by 120°. We obtained 10 and 105 possible different configurations of the [DBUH][TfO] and [DBUH][TFSI] ionic couples, respectively. All these possible configurations were afterwards optimized by means of DFT calculations with the ωB97X-D functional and the 6-31G** basis set, in order to obtain their relative energy. The presence of a polar solvent (dimethylformamide, ε_r = 37.22) was considered, as it was proven in the previous literature that the occurrence of a polarizable medium is a key ingredient to simulate the ionic couples composing ionic liquids [38]. For all configurations of the [DBUH][TfO] ionic couple and for the eight lowest energy configurations of the [DBUH][TFSI] couple the infrared vibration frequencies and intensities were calculated at the same level of theory. In the following we will report only configurations with all positive frequencies and an energy difference of no>11 kJ/mol with respect to the lowest one in order to have an appreciable population. A theoretical absorbance spectrum was obtained by summing Gaussian curves centered at each calculated vibration frequency, with a 10 cm^{-1}standard deviation and an intensity proportional to the calculated one.

3. Results and Discussion

Chemical physical properties of neat DBU [39-41] and [DBUH][TFSI] [8,9,14,42] have been studied in the past by different groups. The conductivity vs. temperature dependence of [DBUH][TFSI], reported in Fig. 1, displays conduction values lower than 10^{-8} S cm^{-1} (i.e., not reported in Fig. 1 as they are below the minimum value detectable by the equipment) from −40 up to 25 °C. The step increase of about four orders of magnitude, recorded above 30 °C, corresponds to the melting of the [DBUH][TFSI] sample, in agreement with the DSC results reported by Watanabe and co-workers (small deviations might be due to different levels of water contamination) [9]. In the molten state [DBUH][TFSI] display a VTF behaviour, typical of ionic liquid materials [9,43]. Further increase in temperature beyond the melting point leads to a progressive raise in conductivity, due to the convective thermal motions within the ionic liquid medium. In the molten state, ion conduction values approaching or overcoming 10^{-3} S cm^{-1} are exhibited, i.e., lower than those of other IL systems based on the TFSI anion [43,44]. For instance, the much larger steric hindrance of the DBUH cation (in combination with enhanced van der Waals forces) with respect to the tetraalkylammonium, piperidinium, pyrrolidinium and, especially, imidazolium cations, leads to remarkable increase of the PIL viscosity. On the other hand, ionic liquids based on bulky

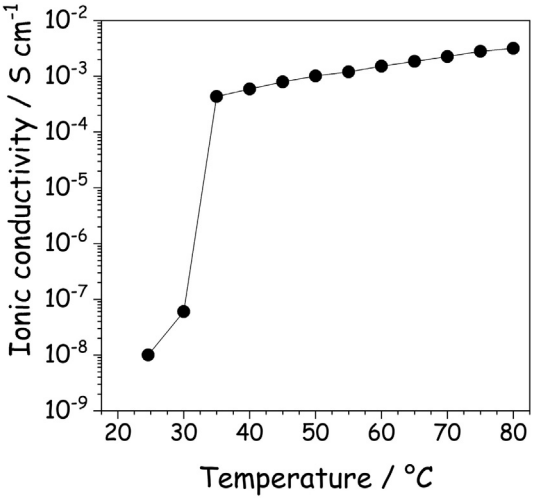

Fig. 1. Conductivity data of [DBUH][TFSI], as a function of temperature.

ions exhibit ion transport properties ionic liquid comparable with those of [DBUH][TFSI]. [44]

The structural features of liquid [DBUH][TFSI] were investigated by the synergy between synchrotron high energy X-ray diffraction and Molecular Dynamics simulation. Our previous study on DBU and other protic ILs based on it showed that the presently used interatomic potential excellently accounts for the structural properties of these systems [12]. The simulated densities are in agreement with experimentally available data sets. In particular we obtain simulated densities of 1.016 g/cc for neat DBU at 298 K [12] and 1.445 g/cc for [DBUH][TFSI] at 303 K to be compared with experimental results: 1.0135 for DBU [45] and 1.4480 g/cc for [DBUH][TFSI] [42]. This agreement is comparable to the one that we previously reported in our simulations of [DBUH][TfO] and [DBUH][IM14] [12]. Therein we also compared experimental X-ray scattering patterns with computed ones for neat DBU and for [DBUH][TfO] and [DBUH][IM14] [12]. In the present case, as [DBUH][TFSI] melts at 25 °C, we could obtain experimental X-ray scattering data at 30 °C. In Fig. 2 we report the comparison between experimental and computed X-ray scattering patterns for [DBUH][TFSI] at 30 °C. In **Figure S1** of the Supporting Information, we also show the previously reported comparison between experimental and computed X-ray scattering patterns, together with the new experimental and computed X-ray scattering pattern from [DBUH][TFSI]. It appears that analogously to the case of [DBUH][IM14] [12], [DBUH][TFSI] is characterised by a scattering feature centred at about 0.85 $Å^{-1}$, that is not present in the case of neat DBU or [DBUH][TfO]. This is a common feature for the case of ionic liquids bearing imide anions such as [TFSI] [46-50] or [IM14] [51-54] and rarely encountered in the case of ILs with other anions. Notably, similarly to the other [DBUH]-based ILs, no evidences of low Q scattering features can be detected, indicating that no extended intermediate range order occurs in this IL [55-57].

On the basis of the X-ray scattering pattern validation of the MD descriptive capability of structural features in [DBUH][TFSI], we next interrogated the Molecular Dynamics simulations on microscopic details of structural correlations in liquid [DBUH][TFSI].

As a preliminary characterization, we explore the inter-ion correlations, showing cation (Cat) / anion (An) (Cat-An), An-An and Cat-Cat centers of mass pair distribution functions. These data are shown in Fig. 3. The observed behaviour is similar to the one found for other [DBUH] based PILs with [TfO] and [IM14] anions, as well as the recently reported behaviour of the PIL [C1hIm][TFSI]

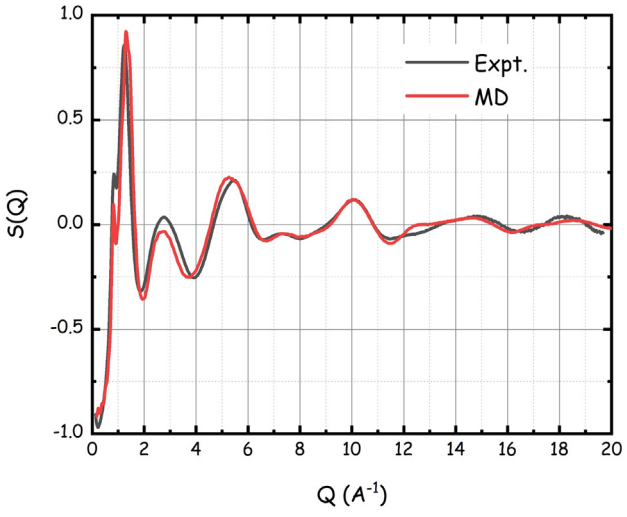

Fig. 2. Experimental (black line) and MD-derived (red line) X-ray scattering patterns for [DBUH][TFSI] at 30 °C.

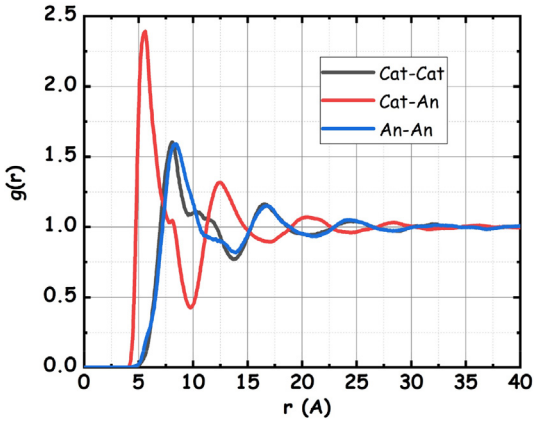

Fig. 3. MD-derived pdfs for CoM sites of the Cation (Cat) and Anion (An) species in [DBUH][TFSI] at 303 K.

[58]. The closest approach is observed for cation–anion correlations at ~ 5.6 Å; the intense first peak shows a shoulder at 8 Å, a feature that was also observed in [DBUH][IM14] [12], although to a lesser extent, and in [C1hIm][TFSI] (at shorter distances) [58]. The first solvation shell is composed of approximately 8 moieties surrounding the oppositely charged species, a value to be compared with 7 and 6, in the cases of [DBUH][TfO] and [DBUH][IM14], respectively. One can rationalise this observation considering that [DBUH][TFSI] is characterised by a larger cation–anion solvation shell than [DBUH][TfO], as the first minimum of the Cat-An pdf (see Fig. 3) falls at ca. 10 Å (to be compared with the value of 8.6 Å found in [DBUH][TfO] [12]).

Moreover, in **Figure S2** of the Supporting Information, we report the spatial distribution functions of [TfO] and [TFSI] anions around a reference [DBUH] cation for the first solvation shell. In the case of the [TfO] anion, the negative charge is more localised and, accordingly, a higher degree of directionality is found in the interaction with the cation, as evidenced by the existence of several coordination lobes in the SDF. On the other hand, charge is more uniformly distributed in [TFSI] and, consequently, one observes a more homogeneous anion distribution around the reference cation (**Figure S2** of the Supporting Information).

Similarly charged species (Cat-Cat and An-An) correlations are characterised by a main peak centred at 8 Å and by a distinct shoulder at about 12 Å and have a similar trend, especially above 14 Å, thus reproducing the common out of phase behaviour with oppositely charged species correlations. Anion-Anion correlations are reported in **Figure S3** of the Supporting Information for the three anions (Tfo, TFSI and IM14) for comparison purposes. Therein, it emerges that TfO anions can approach each other much more closely than other anions, due to the concomitance of reduced sizes and geometric asymmetry. IM14 anions are those who can approach each other at the longest distance, in the first solvation shell: this effect is due to the very large size of these anions as compared to the other two and to the fluorous nature of its chains that enables extensive dispersive interactions between these tails. TFSI, due to its symmetry and intermediate sizes, has a solvation shell with intermediate sizes with respect to the two other anions.

In order to better visualise the nature of cation solvation, we report in Fig. 4, the Spatial Distribution Function (SDF) of both cations and anions Center of Mass (CoM) around a reference cation. Therein, we use the following scheme: a) red lobes refer to anions surrounding the reference cation up to a distance of 7 Å; b) pink lobes refer to anions surrounding the reference cation between 7 and 10 Å; c) blue lobes refer to cations surrounding the reference cation up to a distance of 7 Å; d) cyano lobes refer to cations

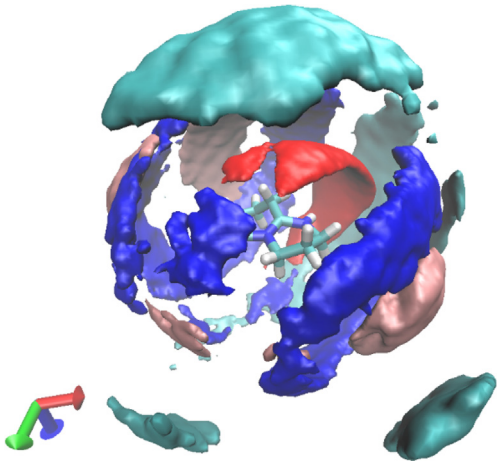

Fig. 4. Spatial Distribution functions of anions (red and pink) and cations (blues and cyan) CoMs solvating a reference cation in [DBUH][TFSI] at 303 K. [Isovalues chosen for the threshold are respectively: 7, 2, 2, 1.5, relative to uniform density]

surrounding the reference cation between 7 and 13.5 Å. It emerges that the closest approach between cation and anions occurs in proximity of the N-H moiety, driven by hydrogen bonding interactions. Further anions building up the first solvation shell create a lantern-like distribution in proximity of the reference cation. First neighbour cations tend to distribute interstitially between this bimodal distribution of anions, occupying space close to the reference cation. Cations, that are more distant, tend to locally neutralise the system, with further intercalation between anions shells. Overall then the main driving force in determining order in this system is hydrogen bonding interactions between opposite ions. Then the trend to locally neutralise charge leads to spatially alternating layers of cations and anions around the reference cation.

In Fig. 5, we show the combined distribution function accounting for the geometrical features of the HB correlation between cation N-H and anion oxygen atoms. It clearly emerges that its length is < 2 Å and it is linear, thus prompting for a HB interaction between ion pairs, similarly to what has been observed for the other [DBUH]-based PILs. In **Figure S4** of the Supporting Information we compare the pair distribution functions for the H···O HB-mediated distance for the two salts [DBUH][TfO] and [DBUH][TFSI]. **Figure S5** of the Supporting Information reports also the number of neighbours extracted from the pair distribution functions for the H···O HB-mediated correlation for comparison with analogous plot reported in ref. [12]. It emerges that both H-bonds are shorter than 2 Å, but the present choice of interatomic potentials prompts for a larger distance for the case of [DBUH][TFSI] than in [DBUH][TfO] ($r^{TFSI}_{H\cdots O}$ = 1.88 Å vs $r^{TfO}_{H\cdots O}$ = 1.78 Å). The same behaviour has been found for the comparison between [DBUH][TfO] and [DBUH][IM14] [12]. These observations are consistent with the proposal from ref. [9] that due to the difference in ΔpKa between [DBUH][TfO] and [DBUH][TFSI] (20.4 vs. 23.4, respectively), a weaker interaction between protonated cation and anion is expected for the case of the [TFSI] anion, as compared to the [TfO] case.

Aiming at further exploring the nature of hydrogen bonding in [DBUH][TFSI], we exploited far-infrared spectroscopy measurements to detect such interactions. Indeed, the spectral range below 200 cm^{-1} can display bands corresponding to the stretching and bending of the hydrogen bonds [38,59]. The far-infrared spectrum of [DBUH][TFSI], measured upon heating between 160 and 340 K, is reported in Fig. 6 in the wavenumber range between 40 and 190 cm^{-1}, where possible markers of hydrogen bonding correlations are expected. At the highest temperatures (T ≥ 300 K), only a broad band centred around 80 cm^{-1} is visible. On the other hand, below T = 280 K, i.e. in the solid phase, one can discern the presence of two well detectable bands around 55 and 90 cm^{-1}as well as a less prominent feature at ca. 110 cm^{-1}, which becomes more evident at lower temperatures. When hydrogen bonding interactions occur in ionic liquids, according to a well established model [38,59], one can decompose the broad band occurring below 150–200 cm^{-1} in at least three contributions: a central band due to dispersion forces, usually centred around 80 cm^{-1}, and two side bands due to the hydrogen bonding bending and stretching modes, usually centred in the ranges 50–70 cm^{-1} and 100–150 cm^{-1}, respectively. [38,59]. The logarithm of the ratio of the intensity of the bands due to a) hydrogen bonding, I_{HB}, and b) dispersion forces, I_{disp}, is supposed to follow the van't Hoff equation, so that by defining $r = \frac{I_{HB}}{I_{disp}}$, one has:

$$\ln(r) = -\frac{1}{T}\frac{\Delta H}{R} + \frac{\Delta S}{R} + c$$

where T is the absolute temperature, R is the gas constant, ΔH and ΔS are the enthalpy and entropy differences between the configurations governed by dispersion forces and by hydrogen bonding, c is a

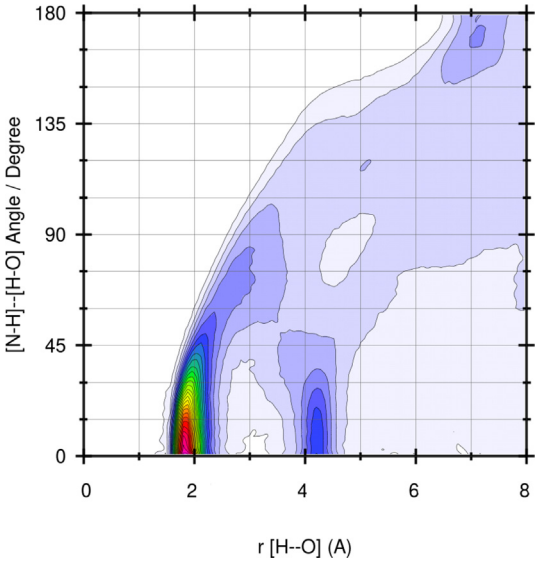

Fig. 5. MD-derived Combined Distribution Function referring to the geometrical features of the hydrogen bonding in [DBUH][TFSI] at 303 K.

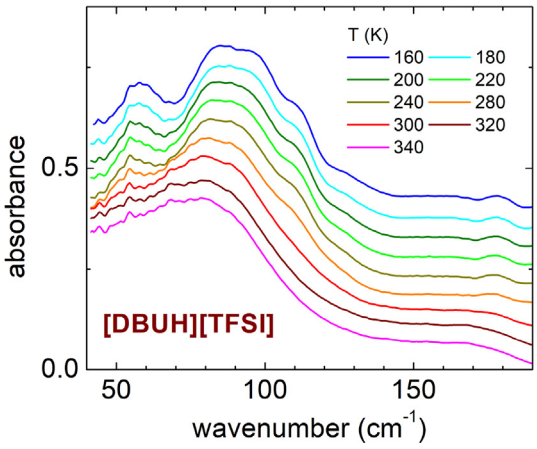

Fig. 6. Temperature dependence of the absorption spectrum of [DBUH][TFSI] measured on heating between 160 and 340 K in the far infrared region.

constant. Therefore, the slope of the linear regression of ln(r) vs 1/T provides a measure of the enthalpy difference between the H-bonded and non H-bonded configurations.

This approach was applied to explore the temperature dependence of the far-IR spectrum of [DBUH][TFSI], by deconvoluting the spectrum using different Lorentzian peaks. A representative decomposition of the broad features observed below 150 cm^{-1} in liquid [DBUH][TFSI]is shown in Fig. 7. At all temperatures the number of contributions to the absorbance was kept to the minimum number of three, in order to avoid data over-interpretation. The van't Hoff plot of ln(r) vs. $1/T$ is displayed in Fig. 8 over the whole probed temperature range, considering the ratio between the intensity of the band centred around 110 and 85 cm^{-1}, due to hydrogen bond stretching and dispersion forces, respectively. The band centred around 50 cm^{-1}, which is located close to the lower limit of the experimental measurements was not further considered for the evaluation of ΔH, as it is more affected by uncertainties. Indeed, the calculated uncertainties of the ratio between the intensities of the band around 85 and 55 cm^{-1} are so high that this quantity is not useful to provide information about the hydrogen bonding. More precise and useful results can be obtained by the ratio of the intensities of the bands centered around 85 and 110 cm^{-1}, as reported in the following.

One can observe two different temperature dependences for ln (r) in the solid and liquid phase. In the solid phase, an Arrhenius-like linear trend is observed between ln(r) and 1/T and one obtains ΔH = 1.9 ± 0.2 kJ/mol, a quite low value. In the liquid phase (1000/T < 3.4 K^{-1}), the intensity of the peak due the hydrogen bond stretching drastically decreases and becomes hardly distinguishable above the intense background and results in a remarkable increase of the relative error of the calculated r values. For this reason, the presently reported infrared measurements suggest that while the occurrence of hydrogen bonding in [DBUH][TFSI] is well evident in the solid phase, HB interactions are hardly detected in the liquid state by means of infrared spectroscopy. This circumstance can be rationalized considering the large geometrical disorder of the liquid phase compared to the solid one and the large number of conformers occurring in the liquid state, which differ in the relative orientation of the N-H. . .O bonds. Indeed, infrared spectroscopy is particularly sensitive to the presence of a good alignment of the hydrogen donor, hydrogen and hydrogen acceptor atoms in order to detect the occurrence of hydrogen bonding stretching bands in the far infrared [38,59].

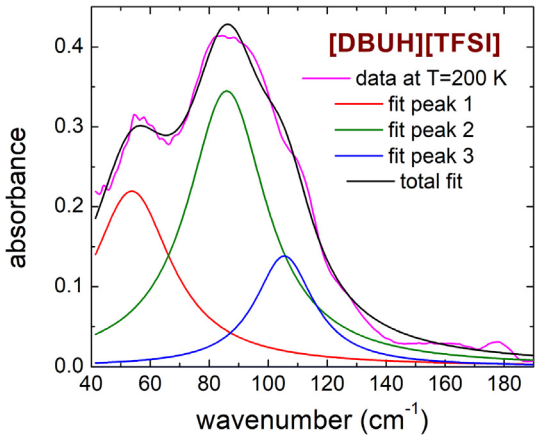

Fig. 7. Typical decomposition of the far-infrared band below 160 cm^{-1}in liquid [DBUH][TFSI]. The contributions attributed to the dispersion forces and to the bending or stretching of the hydrogen bonds are indicated as fit peak 2, 1 and 3, respectively.

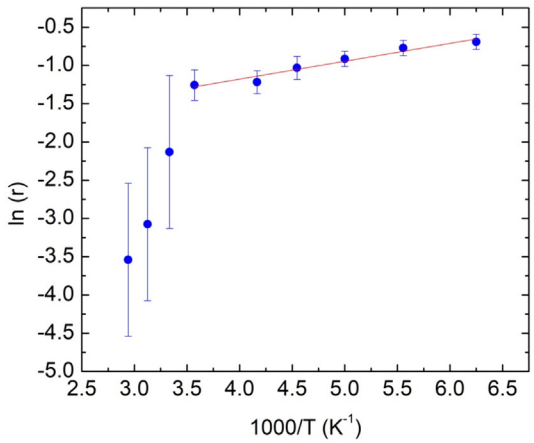

Fig. 8. Van't Hoff plot of the ratio between the intensity of the band centred around 110 and 85 cm^{-1}, due to hydrogen bond stretching and dispersion forces, respectively, in [DBUH][TFSI].

Further support to this hypothesis comes from the comparison of the temperature evolution of the far-infrared spectrum of [DBUH][TFSI] and [DBUH][TfO] and the DFT calculations on the low energy conformers of the two ionic pairs. In the previous literature it was noted that a key role in the presence and in the intensity of the hydrogen bonding is played by the specific anion present in the ionic liquids; therefore, we additionally investigated the far-infrared spectrum of [DBUH][TfO]. Indeed, [TFSI] usually does not give rise to strong hydrogen bonds, while other anions, such as methanesulfonate ([MsO]) and trifluoromethanesulfonate ([TfO]), are more prone to strongly bind to cations [38,59]. Moreover, the [TfO] anion does not possess geometrically different, non-overlapping conformers, so that a liquid containing such an anion

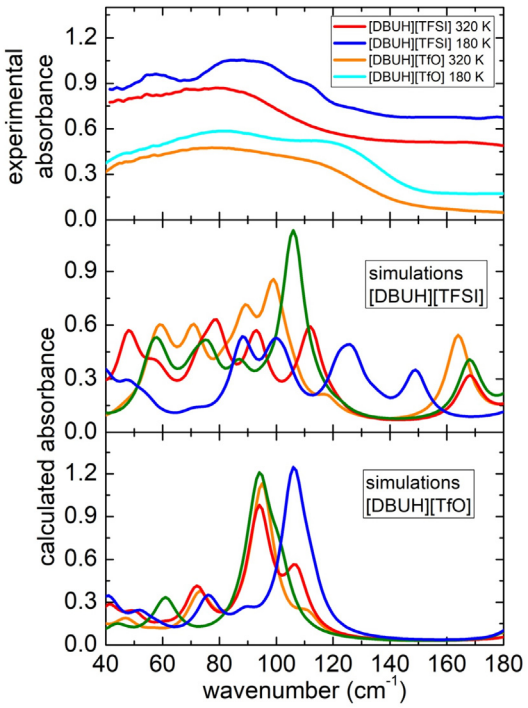

Fig. 9. Comparison of the far-infrared spectra of [DBUH][TFSI] and [DBUH][TfO] measured at 320 K and at 180 K with the calculated absorbance of the four conformers of the ionic couples. For both couples the blue, green, orange and red lines refer to conformer A, B, C and D described in **Figures S6 and S7** of the Supplementary Information, respectively.

should be less affected by geometrical disorder. Fig. 9 reports the comparison of the far-IR spectra of [DBUH][TFSI] and [DBUH][TfO] at 320 K and at 180 K. As already discussed, [DBUH][TFSI] displays three bands at low temperature centered around 80, 55 and 110 cm^{-1}, attributed to the dispersion forces and to the bending and stretching of hydrogen bonding, respectively. In the liquid phase,[DBUH][TFSI]presents only a broad peak centered around 80 cm^{-1}.

On the contrary, in [DBUH][TfO] one can observe three contributions centred around 50, 80 and 120 cm^{-1}, with attributions similar to those reported for [DBUH][TFSI], both at high and low temperature. In particular, the band centred around 120 cm^{-1}, which is attributed to the hydrogen bond stretching, is clearly visible also in the liquid state (see Fig. 10) and its intensity is comparable to that of the band due to the dispersion forces (centred around 80 cm^{-1}). A stronger hydrogen bonding in [DBUH][TfO] is also witnessed by the higher frequency of the hydrogen bond stretching band in [DBUH][TfO] with respect to [DBUH][TFSI] (122 vs. 105 cm^{-1} at 180 K). Indeed, the previous literature pointed out that the frequency of this mode is higher in systems where hydrogen bonding is stronger [38,59]. The frequency values observed in the present study can be also compared to those of the prototypical protic ionic liquids diethylmethylammonium trifluoromethanesulfonate ([DEMA][TfO]) and diethylmethylammonium methanesulfonate ([DEMA][MsO]), where the hydrogen bond stretching bands are experimentally found around 150 and 160 cm^{-1}, respectively [38]. However, the frequencies of the hydrogen bonding stretching of [DBUH][TFSI] and [DBUH][TfO] samples are rather similar to those of 1-ethyl-3-methylimidazolium trifluoromethanesulfonate ([C2mim][TfO]), 1-ethyl-3-methylimidazolium methanesulphonate ([C2mim][MsO]) and 1-butyl-3-ethylimidazolium methanesulphonate ([C4mim][MsO]) [60]. In all these liquids, the hydrogen bond is weaker than in [DEMA][MsO] and [DEMA][TfO], as it involves the weaker C-H...O hydrogen bond interaction [60]. On the contrary, no hydrogen bonding was revealed in 1-ethyl-2,3-dimethyl imidazolium bis(trifluoromethanesulfonyl)imide ([C2Mmim][TFSI]), and in general it is difficult to evidence hydrogen bonds in [TFSI] based ionic liquids [60]. Nevertheless, hydrogen bonding in samples containing either the [TFSI] or the (bis(fluorosulfonyl)imide) ([FSI]) anions was reported for some ionic liquids containing cations bearing an ether functionalized alkyl chain [61].

DFT calculations on the two ionic couples [DBUH][TFSI] and [DBUH][TfO] can further help to understand the apparent lack of a strong indication of hydrogen bonding in the [TFSI]- containing IL from the far-infrared spectra in the liquid phase. An investigation of the conformers of the two ionic couples was performed by a systematic rotation of the flexible bonds by 120°. **Figures S6 and S7** of the Supplementary Information display the four lowest energy conformers of [DBUH][TFSI] and [DBUH][TfO] with all positive vibration frequencies and an energy not differing>11 kJ/mol from the lowest energy ones. The corresponding shortest N-H...O distance and N-H...O angle are reported both in the **Figures S6 and S7** and in the Supplementary material Tables S1 and S2. All configurations are compatible with the occurrence of hydrogen bonding between the H atom attached to N of the cation and one of the O atoms of the anion. It can be noted that the mean NH...O distance decreases from 1.943 Å in [DBUH][TFSI] to 1.891 Å in [DBUH][TfO]. Fig. 9 reports the calculated absorbance spectra for the eight molecular configurations, compared to the experimental data. It is well evident that in [DBUH][TFSI] the four conformers have very different absorbance spectra, due to the quite different molecular configurations of cation, anion and the relative positions. On the contrary, for [DBUH][TfO] all conformers display a clear isolated absorbance peak centered between 95 and 110 cm^{-1}, that by visual inspection of the movements of the atoms, corresponds to the hydrogen bonding stretching. Moreover, the energy differences between the conformers for the two ILs are quite distinct: in [DBUH][TfO] the two lowest energy conformer are separated by 3.8 kJ/mol, while four conformers are expected within such a value for [DBUH][TFSI] (see **Figures S6 and S7** of Supplementary Information). As expected, for [DBUH][TFSI] these energies are quite close: accordingly, all the four conformers will be appreciably populated and all of them will significantly contribute to the measured spectrum. On the contrary for [DBUH][TfO], the main contribution will stem from the lowest energy conformer and will result to be well detectable in the spectrum. It can be noted that the lowest energy conformer of [DBUH][TfO] display the highest frequency of the hydrogen bonding stretching mode. This can possibly explain the shift of this mode to higher frequency in the experimental spectra measured at low temperature, as the population of the lowest energy conformer is expected to increase at lower temperatures.

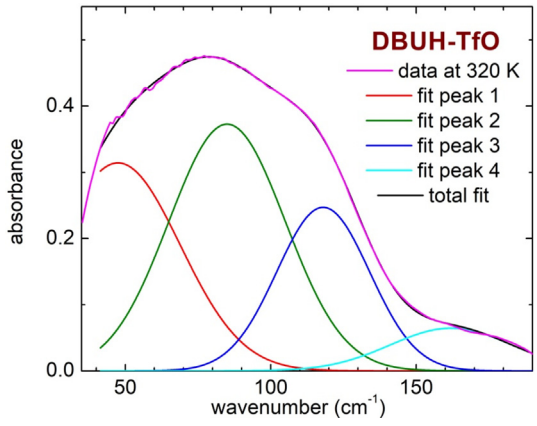

Fig. 10. Typical decomposition of the far infrared band of [DBUH][TfO] in its liquid state with Lorentzian contributions.

4. Conclusion

A super-strong base [DBU]-based PIL was prepared by mixing DBU with the super strong acid, bis(trifluoromethanesulfonyl)-imide, (TFSIH), ([DBUH][TFSI]). The high ΔpKa value for this PIL drives a full proton transfer in the acid-base equilibrium. The microscopic structure of [DBUH][TFSI] was described using a synergy of high energy X-ray scattering and Molecular Dynamics simulation, probing intermolecular interactions at atomistic level. Long range correlations of coulombic nature (leading to a characteristic cation/anion alternation), as well as cation stacking can be observed in the bulk structure. Moreover, the specific role of hydrogen bonding (HB) in determining local correlations has been highlighted. HB geometrical features have been compared with those of recently published [DBUH]-based PILs: following the ΔpKa trend, it emerges that in [DBUH][TFSI], HB are weaker than in [DBUH][TfO]. Such a behaviour has been rationalised by inspection of synchrotron far-IR spectra, as a function of temperature for both PILs. Supporting DFT calculations evidence the importance of low energy stable conformers in determining experimentally derived spectra. In particular, it can be noted that the large conformational disorder present in the liquid phase of [DBUH][TFSI] prevents a clear and direct observation of the hydrogen bonding stretching in the Far-IR spectra, contrary to the case of liquid [DBUH][TfO], where instead it can be clearly detected. In the solid phase of both compounds, the conformational disorder decreases and the HB

stretching absorptions are observable around 122 and 105 cm^{-1} at 180 K in [DBUH][TfO] and [DBUH][TFSI], respectively.

CRediT authorship contribution statement

Alessandro Triolo: Conceptualization, Data curation, Investigation, Methodology, Visualization, Writing – original draft, Writing – review & editing. **Annalisa Paolone:** Conceptualization, Funding acquisition, Investigation, Methodology, Visualization, Writing – original draft. **Angelo Sarra:** Data curation, Formal analysis, Investigation. **Francesco Trequattrini:** Data curation, Formal analysis, Investigation. **Oriele Palumbo:** Conceptualization, Data curation, Investigation. **Giovanni BattistaAppetecchi:** Investigation, Writing – original draft. **Fabrizio Lo Celso:** Data curation, Investigation, Visualization, Writing – original draft. **Philip Chater:** Data curation, Investigation. **Olga Russina:** Conceptualization, Investigation, Project administration, Resources, Supervision, Writing – review & editing.

Declaration of Competing Interest

The authors declare that they have no known competing financial interests or personal relationships that could have appeared to influence the work reported in this paper.

Acknowledgements

This work has been supported by the University of Rome Sapienza Projects: RG11715C7CC660BE and RM120172B2165468. We thank Diamond Light Source for access to beamline I15-1 (CY27222-1).We wish to thank P. Roy and J. B. Brubach of the AILES beamline of Soleil Synchrotron for their help during the beamtime. Part of the research leading to this result has been supported by the project CALIPSOplus under the Grant Agreement 730872 from the EU Framework Programme for Research and Innovation HORIZON 2020, for the beamtime 20190321 at Soleil Synchrotron.

Appendix A. Supplementary material

Supplementary data to this article can be found online at https://doi.org/10.1016/j.molliq.2021.117981.

References

[1] T.L. Greaves, C.J. Drummond, Protic ionic liquids: properties and applications, Chem. Rev. 108 (2008) 206–237.
[2] S. Gabriel, J. Weiner, Ueber einige Abkömmlinge des Propylamins, Berichte der Dtsch. Chem. Gesellschaft 21 (1888) 2669–2679.
[3] P. Walden, Molecular weights and electrical conductivity of several fused salts, Bull. Acad. Imp. Sci. Saint Petersbg. 1800 (1914) 405–422.
[4] S. Lee, A. Ogawa, M. Kanno, H. Nakamoto, T. Yasuda, M. Watanabe, Nonhumidified Intermediate Temperature Fuel Cells Using Protic Ionic Liquids 4 (2010) 9764–9773.
[5] M.A.B.H. Susan, A. Noda, S. Mitsushima, M. Watanabe, Brønsted acid–base ionic liquids and their use as new materials for anhydrous proton conductors, Chem. Commun. 3 (2003) 938–939.
[6] M. Yoshizawa, W. Xu, C.A. Angell, Ionic Liquids by Proton Transfer: Vapor Pressure, Conductivity, and the Relevance of ΔpKa from Aqueous Solutions, J. Am. Chem. Soc. 125 (2003) 15411–15419.
[7] R. Kanzaki, K. Uchida, S. Hara, Y. Umebayashi, S.I. Ishiguro, S. Nomura, Acid-base property of ethylammonium nitrate ionic liquid directly obtained using ion-selective field effect transistor electrode, Chem. Lett. 36 (2007) 684–685.
[8] M.S. Miran, H. Kinoshita, T. Yasuda, M.A.B.H. Susan, M. Watanabe, Hydrogen bonds in protic ionic liquids and their correlation with physicochemical properties, Chem. Commun. 47 (2011) 12676.
[9] M.S. Miran, H. Kinoshita, T. Yasuda, M.A.B.H. Susan, M. Watanabe, Physicochemical properties determined by ΔpK a for protic ionic liquids based on an organic super-strong base with various Brønsted acids, Phys. Chem. Chem. Phys. 14 (2012) 5178–5186.
[10] M.S. Miran, M. Hoque, T. Yasuda, S. Tsuzuki, K. Ueno, M. Watanabe, Key factor governing the physicochemical properties and extent of proton transfer in protic ionic liquids: Δp: K a or chemical structure?, Phys Chem. Chem. Phys. 21 (2019) 418–426.
[11] J.W. Wiench, L. Stefaniak, E. Grech, E. Bednarek, Two amidine derivatives studied by 1H, 13C, 14N, 15N NMR and GIAO-CHF calculations, J. Chem. Soc. Perkin Trans. 2 (1999) 885–889.
[12] A. Triolo, F. Lo Celso, C. Ottaviani, P. Ji, G.B. Appetecchi, F. Leonelli, D.S. Keeble, O. Russina, Structural features of selected protic ionic liquids based on a super-strong base, Phys. Chem. Chem. Phys. 21 (2019) 25369–25378.
[13] L.L. Tolstikova, B.A. Shainyan, Ionic liquids on the basis of 2,3,4,6,7,8,9,10-octahydropyrimido-[1,2-a]azepine (1,8-diazabicyclo[5.4.0]undec-7-ene), Russ. J. Org. Chem. 42 (2006) 1068–1074.
[14] L. L. Tolstikova, A. V. Bel'Skikh and B. A. Shainyan, Trifluoromethanesulfonate, trifluromethylsulfonylimide, and bis(trifluoromethylsulfonyl)imide salts and ionic liquids based on 1,8-diazabicyclo[5.4.0]undec-7-ene and 1,5-diazabicyclo[4.3.0]non-5-ene, *Russ.* J. Org. Chem., 2010, **46**, 383–388.
[15] M. Montanino, F. Alessandrini, S. Passerini, G.B. Appetecchi, Water-based synthesis of hydrophobic ionic liquids for high-energy electrochemical devices, Electrochim. Acta 96 (2013) 124–133.
[16] J. Filik, A.W. Ashton, P.C.Y. Chang, P.A. Chater, S.J. Day, M. Drakopoulos, M.W. Gerring, M.L. Hart, O.V. Magdysyuk, S. Michalik, A. Smith, C.C. Tang, N.J. Terrill, M.T. Wharmby, H. Wilhelm, Processing two-dimensional X-ray diffraction and small-angle scattering data in DAWN 2, J. Appl. Crystallogr. 50 (2017) 959–966.
[17] A.K. Soper, E.R. Barney, Extracting the pair distribution function from white-beam X-ray total scattering data, J. Appl. Crystallogr. 44 (2011) 714–726.
[18] A.K. Soper, The Radial Distribution Functions of Water as Derived from Radiation Total Scattering Experiments: Is There Anything We Can Say for Sure?, ISRN Phys Chem. 2013 (2013) 1–67.
[19] B. Hess, C. Kutzner, D. van der Spoel, E. Lindahl, GROMACS 4: Algorithms for Highly Efficient, Load-Balanced, and Scalable Molecular Simulation, J. Chem. Theory Comput. 4 (2008) 435–447.
[20] D. Van Der Spoel, E. Lindahl, B. Hess, G. Groenhof, A.E. Mark, H.J.C. Berendsen, GROMACS: Fast, flexible, and free, J. Comput. Chem. 26 (2005) 1701–1718.
[21] J.N. Canongia Lopes, A.A.H. Padua, Molecular Force Field for Ionic Liquids Composed of Triflate or Bistriflylimide Anions, J. Phys. Chem. B 108 (2004) 16893–16898.
[22] K. Shimizu, D. Almantariotis, M.F.C. Gomes, A.A.H. Pádua, J.N. Canongia Lopes, Molecular Force Field for Ionic Liquids V: Hydroxyethylimidazolium, Dimethoxy-2- Methylimidazolium, and Fluoroalkylimidazolium Cations and Bis(Fluorosulfonyl)Amide, Perfluoroalkanesulfonylamide, and Fluoroalkylfluorophosphate Anions, J. Phys. Chem. B 114 (2010) 3592–3600.
[23] A.K. Malde, L. Zuo, M. Breeze, M. Stroet, D. Poger, P.C. Nair, C. Oostenbrink, A.E. Mark, An Automated force field Topology Builder (ATB) and repository: Version 1.0, J. Chem. Theory Comput. 7 (2011) 4026–4037.
[24] W.L. Jorgensen, D.S. Maxwell, J. Tirado-Rives, Development and Testing of the OPLS All-Atom Force Field on Conformational Energetics and Properties of Organic Liquids, J. Am. Chem. Soc. 118 (1996) 11225–11236.
[25] C.E.S. Bernardes, A. Joseph, Evaluation of the OPLS-AA Force Field for the Study of Structural and Energetic Aspects of Molecular Organic Crystals, J. Phys. Chem. A 119 (2015) 3023–3034.
[26] L. Martínez, R. Andrade, E.G. Birgin, J.M. Martínez, PACKMOL: A package for building initial configurations for molecular dynamics simulations, J. Comput. Chem. 30 (2009) 2157–2164.
[27] G. Bussi, D. Donadio and M. Parrinello, Canonical sampling through velocity rescaling, J. Chem. Phys. DOI:10.1063/1.2408420.
[28] M. Parrinello, A. Rahman, Polymorphic transitions in single crystals: A new molecular dynamics method, J. Appl. Phys. 52 (1981) 7182–7190.
[29] T. Darden, D. York, L. Pedersen, Particle mesh Ewald: An N·log(N) method for Ewald sums in large systems, J. Chem. Phys. 98 (1993) 10089–10092.
[30] U. Essmann, L. Perera, M.L. Berkowitz, T. Darden, H. Lee, L.G. Pedersen, A smooth particle mesh Ewald method, J. Chem. Phys. 103 (1995) 8577–8593.
[31] J.D. Hunter, Matplotlib: A 2D graphics environment, Comput. Sci. Eng. 9 (2007) 90–95.
[32] W. Humphrey, A. Dalke, K. Schulten, VMD: Visual molecular dynamics, J. Mol. Graph. 14 (1996) 33–38.
[33] H.K. Kashyap, J.J. Hettige, H.V.R. Annapureddy, C.J. Margulis, SAXS anti-peaks reveal the length-scales of dual positive–negative and polar–apolar ordering in room-temperature ionic liquids, Chem. Commun. 48 (2012) 5103.
[34] O. Hollóczki, M. Macchiagodena, H. Weber, M. Thomas, M. Brehm, A. Stark, O. Russina, A. Triolo, B. Kirchner, Triphilic Ionic-Liquid Mixtures: Fluorinated and Non-fluorinated Aprotic Ionic-Liquid Mixtures, ChemPhysChem 16 (2015) 3325–3333.
[35] M. Brehm, B. Kirchner, TRAVIS - A Free Analyzer and Visualizer for Monte Carlo and Molecular Dynamics Trajectories, J. Chem. Inf. Model. 51 (2011) 2007–2023.
[36] M. Brehm, M. Thomas, S. Gehrke, B. Kirchner, TRAVIS—A free analyzer for trajectories from molecular simulation, J. Chem. Phys. 152 (2020) 164105.
[37] Y. Shao, L. F. Molnar, Y. Jung, J. Kussmann, C. Ochsenfeld, S. T. Brown, A. T. B. Gilbert, L. V. Slipchenko, S. V. Levchenko, D. P. O'Neill, R. A. DiStasio Jr, R. C. Lochan, T. Wang, G. J. O. Beran, N. A. Besley, J. M. Herbert, C. Yeh Lin, T. Van Voorhis, S. Hung Chien, A. Sodt, R. P. Steele, V. A. Rassolov, P. E. Maslen, P. P. Korambath, R. D. Adamson, B. Austin, J. Baker, E. F. C. Byrd, H. Dachsel, R. J. Doerksen, A. Dreuw, B. D. Dunietz, A. D. Dutoi, T. R. Furlani, S. R. Gwaltney, A. Heyden, S. Hirata, C.-P. Hsu, G. Kedziora, R. Z. Khalliulin, P. Klunzinger, A. M. Lee, M. S. Lee, W. Liang, I. Lotan, N. Nair, B. Peters, E. I. Proynov, P. A. Pieniazek, Y. Min Rhee, J. Ritchie, E. Rosta, C. David Sherrill, A. C. Simmonett, J. E.

Subotnik, H. Lee Woodcock III, W. Zhang, A. T. Bell, A. K. Chakraborty, D. M. Chipman, F. J. Keil, A. Warshel, W. J. Hehre, H. F. Schaefer III, J. Kong, A. I. Krylov, P. M. W. Gill and M. Head-Gordon, Advances in methods and algorithms in a modern quantum chemistry program package, Phys. Chem. Chem. Phys., 2006, **8**, 3172–3191.

[38] O. Palumbo, A. Cimini, F. Trequattrini, J.-B. Brubach, P. Roy, A. Paolone, The infrared spectra of protic ionic liquids: performances of different computational models to predict hydrogen bonds and conformer evolution, Phys. Chem. Chem. Phys. 22 (2020) 7497–7506.

[39] A. Ostonen, E. Sapei, P. Uusi-Kyyny, A. Klemelä, V. Alopaeus, Measurements and modeling of CO_2 solubility in 1,8-diazabicyclo-[5.4.0]-undec-7-ene-Glycerol solutions, Fluid Phase Equilib. 374 (2014) 25–36.

[40] S. Lin, H. Lu, Y. Liu, C. Liu, B. Liang, K. Wu, Density studies of 1,8-diazabicyclo [5.4.0]undec-7-ene (DBU)-glycerol and CO2-DBU-glycerol solutions at temperatures between 288.15 K and 328.15 K, J. Chem. Thermodyn. 123 (2018) 8–16.

[41] Y. Liu, S. Lin, H. Lu, C. Liu, K. Wu, W. Jiang, B. Liang, Studies on viscosity and conductivity of 1,8-diazabicyclo[5.4.0]undec-7-ene (DBU)-glycerol and CO 2 -DBU-glycerol solutions at temperatures from 288.1 K to 328.1 K, J. Chem. Thermodyn. 136 (2019) 16–27.

[42] M.S. Miran, T. Yasuda, M.A.B.H. Susan, K. Dokko, M. Watanabe, (Keynote) Protic Ionic Liquids Based on a Super-Strong Acid: Bulk and Electrochemical Properties, ECS Trans. 50 (2013) 285–291.

[43] M. Montanino, M. Carewska, F. Alessandrini, S. Passerini and G. B. Appetecchi, in *Electrochimica Acta*, Elsevier Ltd, 2011, vol. 57, pp. 153–159.

[44] G.B. Appetecchi, M. Montanino, M. Carewska, M. Moreno, F. Alessandrini, S. Passerini, Chemical–physical properties of bis(perfluoroalkylsulfonyl)imide-based ionic liquids, Electrochim. Acta 56 (2011) 1300–1307.

[45] S. Lin, H. Lu, Y. Liu, C. Liu, B. Liang, K. Wu, Density studies of 1,8-diazabicyclo [5.4.0]undec-7-ene (DBU)-glycerol and CO 2 -DBU-glycerol solutions at temperatures between 288.15 K and 328.15 K, J. Chem. Thermodyn. 123 (2018) 8–16.

[46] O. Russina, A. Triolo, L. Gontrani, R. Caminiti, D. Xiao, L.G. Hines Jr, R.A. Bartsch, E.L. Quitevis, N. Pleckhova, K.R. Seddon, Morphology and intermolecular dynamics of 1-alkyl-3-methylimidazolium bis{(trifluoromethane)sulfonyl} amide ionic liquids: structural and dynamic evidence of nanoscale segregation, J. Phys. Condens. Matter 21 (2009) 424121.

[47] A. Triolo, O. Russina, B. Fazio, G. B. Appetecchi, M. Carewska and S. Passerini, Nanoscale organization in piperidinium-based room temperature ionic liquids, J. Chem. Phys., , DOI:10.1063/1.3119977.

[48] H. K. Kashyap, C. Santos, N. S. Murthy, J. J. Hettige, K. Kerr, S. Ramati, J. Gwon, M. Gohdo, S. I. Lall-, J. F. Wishart, C. J. Margulis and E. W. Castner, Structure of 1-Alkyl-1-methylpyrrolidinium Bis (trifluoromethylsulfonyl) amide Ionic Liquids with Linear , Branched and Cyclic Alkyl Groups, , DOI:10.1021/jp403518j.

[49] E. Bodo, L. Gontrani, R. Caminiti, N.V. Plechkova, K.R. Seddon, A. Triolo, Structural Properties of 1-Alkyl-3-methylimidazolium Bis {(trifluoromethyl)sulfonyl}amide Ionic Liquids: X-ray Diffraction Data and Molecular Dynamics Simulations, J. Phys. Chem. B 114 (2010) 16398–16407.

[50] O. Russina, A. Triolo, New experimental evidence supporting the mesoscopic segregation model in room temperature ionic liquids, Faraday Discuss. 154 (2012) 97–109.

[51] O. Russina, F. Lo Celso, M. Di Michiel, S. Passerini, G.B. Appetecchi, F. Castiglione, A. Mele, R. Caminiti, A. Triolo, Mesoscopic structural organization in triphilic room temperature ionic liquids, Faraday Discuss. 167 (2013) 499.

[52] F. Lo Celso, Y. Yoshida, R. Lombardo, C. Jafta, L. Gontrani, A. Triolo, O. Russina, Mesoscopic structural organization in fluorinated room temperature ionic liquids, Comptes Rendus Chim. 21 (2018) 757–770.

[53] F. Lo Celso, G.B. Appetecchi, E. Simonetti, U. Keiderling, L. Gontrani, A. Triolo, O. Russina, Mesoscopic structural organization in fluorinated pyrrolidinium-based room temperature ionic liquids, J. Mol. Liq. 289 (2019) 111110.

[54] F. Lo Celso, G.B. Appetecchi, E. Simonetti, M. Zhao, E.W.C. Jr, U. Keiderling, L. Gontrani, A. Triolo, Microscopic Structural and Dynamic Features in Triphilic Room Temperature Ionic Liquids 7 (2019) 1–14.

[55] A. Triolo, O. Russina, H.J. Bleif, E. Di Cola, Nanoscale segregation in room temperature ionic liquids, J. Phys. Chem. B 111 (2007) 4641–4644.

[56] O. Russina, F. Lo Celso, N.V. Plechkova, A. Triolo, Emerging Evidences of Mesoscopic-Scale Complexity in Neat Ionic Liquids and Their Mixtures, J. Phys. Chem. Lett. 8 (2017) 1197–1204.

[57] S. Marullo, F. D'Anna, C. Rizzo, F. Billeci, Ionic liquids: "normal" solvents or nanostructured fluids?, Org Biomol. Chem. 19 (2021) 2076–2095.

[58] H. Watanabe, H. Doi, S. Saito, M. Matsugami, K. Fujii, R. Kanzaki, Y. Kameda, Y. Umebayashi, Hydrogen bond in imidazolium based protic and aprotic ionic liquids, J. Mol. Liq. 217 (2016) 35–42.

[59] K. Fumino, V. Fossog, P. Stange, D. Paschek, R. Hempelmann, R. Ludwig, Controlling the subtle energy balance in protic ionic liquids: Dispersion forces compete with hydrogen bonds, Angew. Chemie - Int. Ed. 54 (2015) 2792–2795.

[60] O. Palumbo, A. Cimini, F. Trequattrini, J.-B. Brubach, P. Roy, A. Paolone, Evidence of the CH···O HydrogenBonding in Imidazolium-Based Ionic Liquids from Far-Infrared Spectroscopy Measurements and DFT Calculations, Int. J. Mol. Sci. 22 (2021) 6155.

[61] O. Palumbo, F. Trequattrini, A. Cimini, A. Tsurumaki, M.A. Navarra, A. Paolone, Inter- and Intramolecular Interactions in Ether-Functionalized Ionic Liquids, J. Phys. Chem. B 125 (2021) 2380–2388.